Aromaticity balance, π-electron cooperativity and H-bonding properties in tautomerism of salicylideneaniline: The quantum theory of atoms in molecules (QTAIM) approach

ARTICLE *in* JOURNAL OF MOLECULAR MODELING · JUNE 2011

Impact Factor: 1.74 · DOI: 10.1007/s00894-010-0832-3 · Source: PubMed

4 AUTHORS, INCLUDING:

Hasan Karabıyık
Dokuz Eylul University
40 PUBLICATIONS **234** CITATIONS
SEE PROFILE

Resul Sevinçek
Dokuz Eylul University
20 PUBLICATIONS **38** CITATIONS
SEE PROFILE

Muhittin Aygün
Dokuz Eylul University
80 PUBLICATIONS **327** CITATIONS
SEE PROFILE

J Mol Model (2011) 17:1295–1309
DOI 10.1007/s00894-010-0832-3

ORIGINAL PAPER

Aromaticity balance, π-electron cooperativity and H-bonding properties in tautomerism of salicylideneaniline: the quantum theory of atoms in molecules (QTAIM) approach

Hasan Karabıyık · Resul Sevinçek · Hande Petek · Muhittin Aygün

Received: 7 May 2010 / Accepted: 22 August 2010 / Published online: 5 September 2010

Abstract Topological analysis based on DFT calculations regarding proton transfer reaction in salicylideneaniline (SA) was performed to scrutinize possible changes in the intramolecular H-bond, π-electron delocalization and aromaticity levels of certain fragments. Quantum chemical calculations and natural bond orbital (NBO) analyses were carried out over a tautomeric ensemble whose members correspond to the molecules at different stages in tautomeric interconversion of SA. The elaboration of intramolecular hydrogen bonding in terms of the relevant topological parameters and the interpretation of certain dependencies regarding its strength were examined. The results show that delocalization index (DI) between donor and acceptor atom δ(O,N) is a useful topological parameter for describing H-bond strength, which is influenced by π-delocalization level within quasiaromatic chelate ring, indicating its resonance-assisted character. NBO analyses reveal that lone-pair (LP) population on N center also affects the strength of intramolecular H-bond in SA. Furthermore, π-electron transfer accompanying intramolecular proton migration in SA is brought into being through formally vacant non-Lewis type LP* orbital on the tautomeric proton. As a result of this, tautomeric protons in molecular entities near TS have hypovalent character due to the lack of electron population in the bonding orbital relative to that in LP* orbital. While H-bonds in the tautomeric ensemble of SA are predominantly partial covalent, molecular entities close to transition state have the strongest covalent H-bonds. The most important result is also that there are linear correlations between the orders of bonds (hydroxyl and amine) involving intramolecular H-bond and electron density values at the relevant BCPs due to partially covalent character of these bonds, contrary to exponential behavior as for purely covalent bonds. Quasiaromatic chelate ring formation is established not only to compel a reduced aromaticity of salicylidene ring but also to decrease in LP-population on N.

Keywords Aromaticity · Hypervalent · Hypovalent · Intramolecular electron transfer · Para delocalization index · Schiff base

Electronic supplementary material The online version of this article (doi:10.1007/s00894-010-0832-3) contains supplementary material, which is available to authorized users.

H. Karabıyık (✉) · R. Sevinçek · M. Aygün
Department of Physics, Dokuz Eylül University,
35160 İzmir, Turkey
e-mail: hasan.karabiyik@deu.edu.tr

H. Petek
Department of Physics, Ondokuz Mayıs University,
55139 Samsun, Turkey

Introduction

o-hydroxy aromatic Schiff bases have received much attention in many different areas such as biology, coordination chemistry, technological applications and chemical physics [1–4], in particular due to their phenol-keto tautomerism [5, 6]. Depending on the position of the tautomeric proton, two types of intramolecular hydrogen bond involving a photochemically or thermochemically induced proton are possible, namely O—H···N in phenol (OH) and O···H—N in keto (NH) tautomer [7–10]. In general, the latter can be identified as a resonance hybrid of two canonical structures: *cis*-keto tautomer and zwitterionic form, having identical atomic positions but different covalent skeleton [11–15] as shown in Scheme 1. Salicylideneaniline (SA) [16] is an aromatic Schiff bases which has long-ranged π-electron delocalization capacity affecting

whole molecule during the proton transfer reaction, O—H···N ↔ O···H—N [14, 15]. It is obvious that change in π-electron delocalization of SA is a driving force establishing tautomeric equilibrium and intramolecular H-bonding shown in Scheme 1. Heteronuclear intramolecular H-bond in SA is the most intriguing phenomenon due to its resonance-assisted (or charge-assisted) nature and also is of fundamental importance in the theory of hydrogen bonding [17, 18], since π-electron delocalization affects the characteristics and strength of hydrogen bonds [19–26] as well as the acid and base centers [25, 26].

Filarowski and his colleagues have shown that the aromaticity balance plays an important role in stabilizing of tautomeric equilibria of *o*-hydroxy aryl Schiff base species in a series of papers [27–30]. Quasiaromatic chelate ring formation in NH tautomer reduces aromaticity (or π-electron delocalization) in salicylidene ring, reflecting a dynamic balance between aromaticities of these adjacent fragments. In addition, resonance-assisted H-bond (RAHB) affects the electronic state of its neighboring aromatic fragments. Although the inferences by Filarowski and his colleagues about aromaticity balance in tautomerism of *o*-hydroxy aromatic Schiff bases are of great importance in terms of the relevant scientific community and provide useful insights in understanding of π-electron delocalization and common features for such molecules, a reasonable criticism can be directed to these inferences from a statistical point of view. The mentioned dynamics between aromaticity levels in salicylidene ring and chelate moiety (O—C1=C6—C7=N) are obtained from chemically distinct Schiff base species in different crystal structures. These results are not obtained from a tautomeric ensemble whose members correspond to the molecules at different stages of the chemical process such as tautomerism (or self-isomerism) occurring in the same molecule. Experimental attainment of such a tautomeric ensemble for SA by X-ray diffraction method is difficult, since keto and phenol tautomers at different stages in tautomerism of SA may not be sufficiently distinguishable from one another due to positional disorder, in particular for the tautomeric protons located at the midway between O and N in low-barrier H-bonds of such compounds [15].

In the present study, our particular interest will be addressed to extend the concept of aromaticity balance to SA within the relevant tautomeric ensemble and to deepen the considerations for tautomerism in SA, especially the effects from changes in π-electron delocalization accompanying intramolecular proton transfer on covalent topology of SA. Reason for taking into consideration of SA in this study is to eliminate the steric effects playing an important role in tautomerism of *o*-hydroxyaryl Schiff bases [27, 29]. The interconversion between two limiting tautomer (phenol and *cis*-keto) of SA and its effects on the molecular geometry besides electronic redistribution in molecular orbitals were monitored by a relaxed potential energy surface (PES) scan with respect to hydroxyl bond length d(O—H) used as redundant internal coordinate, allowing formation of a tautomeric ensemble for SA. Thus, the aim of this study is to investigate chemical background underlying tautomerism of SA in terms of structural and electronic behaviors.

Computational strategy and methodology

One dimensional relaxed potential energy surface (PES) scan was performed on the basis of the global minimum of phenol form of SA by changing hydroxyl bond length *d*(O—H) as a redundant internal coordinate [31] from 0.90 Å to 1.80 Å in every 0.05 Å. All of the remaining internal coordinates were fully optimized at each point in the scan process according to Berny optimization algorithm [32] by using DFT calculations with the use of Becke's three-parameters hybrid exchange-correlation functional (B3LYP) [33] incorporating B88 gradient-corrected exchange [34] and Lee-Yang-Parr non-

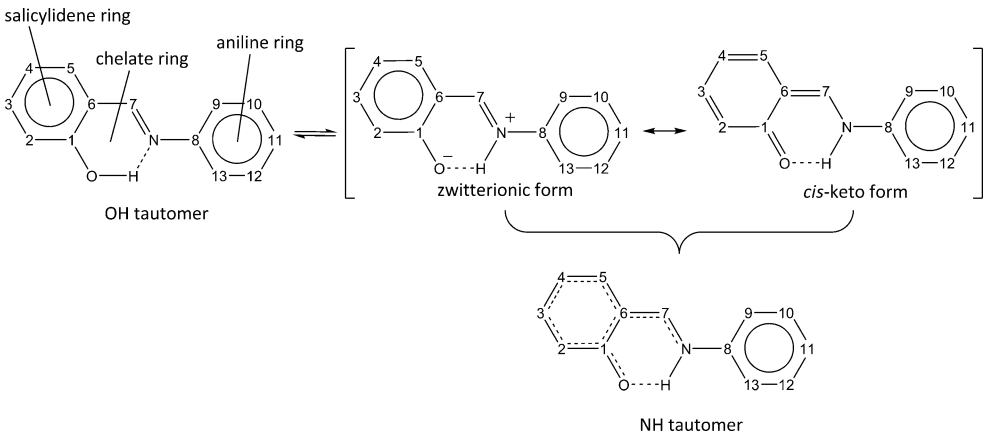

Scheme 1 Tautomeric equilibrium of SA with the atomic numbering scheme for C atoms. The *cis* labeling is based on relative positions of tautomeric H and O in *ortho* position

local correlation functional [35] by means of 6-311++G(d,p) basis set implemented in Gaussian 03 W program package [36]. Thus, a tautomeric ensemble consisting of different molecular geometries in various stages of tautomerism of SA is obtained by PES representing proton transfer process in hydrogen bridge. To able to examine bonding situations and electronic populations in certain natural atomic orbitals, Natural Bond Orbital (NBO) analyses [37–39] were carried out at the same level of theory on the basis of each optimized entities in the tautomeric ensemble under discussion.

In order to quantitatively describe aromaticity of the various molecular fragments in SA, delocalization indices were computed in the framework of the quantum theory of atoms in molecules (QTAIM) [40–42]. Heretofore, different criteria based on electron delocalization measures have been defined for the purpose of quantitative evaluation of aromaticity [43–47]. Other aromaticity measures from distinct origins such as structural, reactivity, special magnetic properties may generate contradictory results, or at least not correlated well with each other [48, 49]. Therefore, the use of delocalization indices (DIs) for investigating aromaticity is beneficial, since they refer directly to the idea of electron delocalization underlying the concept of aromaticity. Recently, para delocalization index (PDI) based on the calculation of the local DIs has become one of the most efficient ways to describe the degree of electron delocalization level [43–47]. PDI is defined as the average of delocalization indices between *para*-related atom pairs,

$$PDI = \frac{1}{3}\sum_{i=1}^{3}\delta(i,i+3) \tag{1}$$

DI between atoms A and B, δ(A,B), is obtained by double integration of exchange or Fermi correlation between electrons, $\Gamma_{xc}(\mathbf{r}_1,\mathbf{r}_2)$, over the atomic basins Ω_i and Ω_j:

$$\delta(i,j) = -2\int_{\Omega_i}\int_{\Omega_j}\Gamma_{xc}(\mathbf{r}_1,\mathbf{r}_2)d\mathbf{r}_1 d\mathbf{r}_2, \tag{2}$$

and can be seen as a quantitative measure of electron pair sharing between atomic basins Ω_i and Ω_j [50]. Equation 2 is rewritten in terms of the overlap between the molecular orbitals k and l within the basin of atom i (Ω_i) by $S_{kl}(\Omega_i)$ as follows;

$$\delta(i,j) = 4\sum_{k,l}^{N/2} S_{kl}(\Omega_i)S_{kl}(\Omega_j), \tag{3}$$

where the summation runs over all $N/2$ occupied molecular orbitals for atoms which have only closed-shell interactions with their neighbors [50]. Wavefunction sets corresponding to the tautomers at each point of PES scan are obtained by Kohn-Sham molecular orbitals. Then, they are used as input data to AIM2000 software [51] to perform topological analyses on the electron density distribution $\rho(\mathbf{r})$ and to calculate the delocalization indices. It is worth noting that DI is closely related to formal bond order between the atom i and j [52], and therefore DI may be indirectly regarded as a measure of π-character of a bond.

Certain points in the electron density where $\nabla\rho(\mathbf{r})$ vanishes are called critical points (CPs), which are further grouped into four classes referred to as (3,−3), (3, −1), (3,+1) and (3,+3). These classes are denoted by the ordered pairs (r,s) denoting their rank (r) and signature (s) defined as an algebraic sum of the signs of the eigenvalues the diagonalized Hessian matrix of $\rho(\mathbf{r})$. CP (3, −1) and (3,+1) are saddle points, called the bond critical point (BCP) and the ring critical point (RCP), respectively. Diagonalization of the Hessian of the electron density at (3, −1) CPs yields three ordered eigenvalues λ_1, λ_2 and λ_3, which denote principal curvatures [53]. BCPs and RCPs in SA were analyzed by QTAIM methodology [40–42], since it is known that the electron density $\rho(\mathbf{r}_{BCP})$ and its Laplacian $\nabla^2\rho(\mathbf{r}_{BCP})$ at the BCP or RCP may be very useful parameters for the estimation of the relative strength of H-bonds [19–24, 54]. At CPs, these topological tools can be connected by the total electronic energy density (H_C) via the following local virial theorem in atomic units,

$$\frac{1}{4}\nabla^2\rho(\mathbf{r}_{CP}) = 2G_C(\mathbf{r}_{CP}) + V_C(\mathbf{r}_{CP}), \qquad H_C = G_C + V_C \tag{4}$$

where V_C and G_C stand for local potential and kinetic electron energy density, respectively [55]. Estimating H-bond dissociation energy E_{HB} is usually an arduous task because of the fact that many different conformers as a result of H-bonding are possible. To describe H-bond dissociation energy in terms of topological functions in the HB region, heretofore two main approaches have been put forward. While the first by Espinosa *et al.* [56] have reported that $-1/2V_C(\mathbf{r}_{BCP})$ correlates well-with E_{HB}, where $V_C(\mathbf{r}_{BCP})$ denotes local electron potential energy density at the BCP between hydrogen and acceptor atom, the second one by Musin & Mariam [57] is disposed to correlate E_{HB} (in kcal mol^{-1}) with the interatomic separation (in Å) from donor (D) to acceptor (A) according to the following empirical relationship,

$$E_{HB} = 5.554 \times 10^5 \exp(-4.12 d_{D\cdots A}). \tag{5}$$

Results and discussion

Structural and energetic remarks

Relative energies of the molecular entities in the tautomeric ensemble of SA with respect to that of the optimized

geometry of SA are shown in Fig. 1. Energy difference between the stable OH (at third step) and NH (at seventeenth step) tautomer is obtained as 4.65 kcal mol^{-1} in gas phase and in well-agreement with the corresponding value (4.6 kcal mol^{-1}) previously reported by Ogawa and Fujiwara [58]. The activation energy of the transition from the global minimum to the local minimum is 6.29 kcal mol^{-1} and this excitation is accompanied by intramolecular proton transfer from the hydroxyl group to the N atom in the ground state. This potential barrier height is comparable with those of *o*-hydroxy aryl Schiff bases species [27–29]. The large curvature of the potential energy for proton transfer in vicinity of the phenol-imine wall (Fig. 1) is associated with a large zero-point energy contribution in the ground state vibrational mode, which destabilizes the phenol-imine form [59]. Because of electronic redistribution during proton transfer, aniline ring rotates around N—C8 axis, ultimately resulting in almost planar molecular geometry for the stable NH tautomer. Rotation of salicylidene ring around C6—C7 axis is prevented by intramolecular H-bond due to chelate ring strain. Another reason is also that C6—C7 bond become increasingly double bond, not allowing the rotation. Thus, it can be stated that chelate ring formation decreases conformational flexibility of salicylidene fragment in SA. Optimized OH geometry of the compound is initially adapted nonplanar geometry with dihedral angle between the rings of 41.08°. Progressing proton transfer process, molecular geometry of SA becomes planar gradually, and the stable NH form appeared at seventeenth step of the scan process is exactly planar as shown in Fig. 2. Planarization of SA has destabilized the parent phenol-imine tautomer by 4.65 kcal mol^{-1}. This can be explained by the increased basicity of N atom in planar conformation [60] preventing

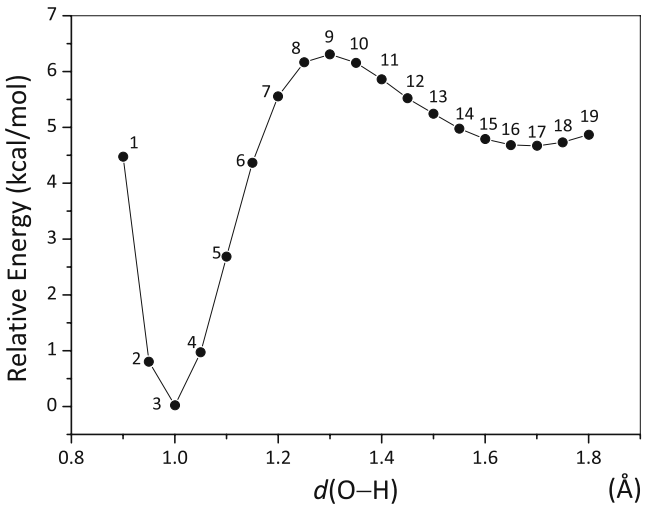

Fig. 1 Potential energy curve for proton transfer reaction in SA with the corresponding step numbers

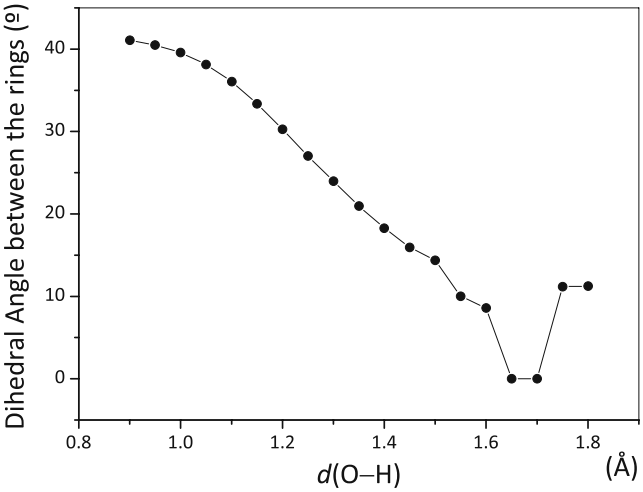

Fig. 2 Dihedral angle between salicylidene and aniline ring against the scan coordinate

the lone-pair (LP) electrons on N to be conjugated with salicylidene ring. This inference is verified by lagrangian values (–0.25 times integral of the Laplacian of the electron density over atomic basin) in N atom for the stable NH and OH tautomers. Lagrangian values of electron density can be connected with the concepts of Lewis acidity and basicity [61]. Lagrangian values of N atoms for the stable OH and NH tautomers are found as 2.265×10^{-5} a.u. and 2.747×10^{-4} a.u. respectively. Since local charge concentration disclosing itself by $\nabla^2\rho<0$ behaves as a Lewis base, thus it can be stated that augmentation in Lagrangian value of N atom indicates an increase in basicity of N atom. Another reason for that planarization of SA makes it less stable may be steric hindrance between H atoms bonded to C7 and C9. The distances between these H atoms in stable OH and NH tautomer are 2.35 Å to 2.10 Å, respectively. In addition, distance between H7 and H9 atoms during the proton transfer reaction remains smaller than the summation of their van der Waals radii [62]. Figure 3 shows three representative members in tautomeric ensemble of SA, stable OH, stable NH and TS with their all CPs. Formation of the chelate ring by RCP and BCPs of hydroxyl and amine bonds are unequivocally seen from Fig. 3. In particular, it should be pointed out that there is a H-H bonding [63] between H7 and H9 in the stable NH form of SA as shown in Fig. 3c. Values of some topological parameters at BCP between H7 and H9 such as ρ, $\nabla^2\rho$, G_C, V_C and bond path length are found as 0.0108, 0.0411, 0.0083, -0.0062 and 4.385 (in a. u.), respectively. These results are in agreement with those reported in [63]. Although the concept of H-H bonding is a speculative phenomenon in the literature [64–66], our results reveal its presence as claimed by Matta *et al.* [63]. In addition, such a H-H bonding makes a stabilizing contribution up to 10 kcal mol^{-1} [63]. Consequently, steric hindrance

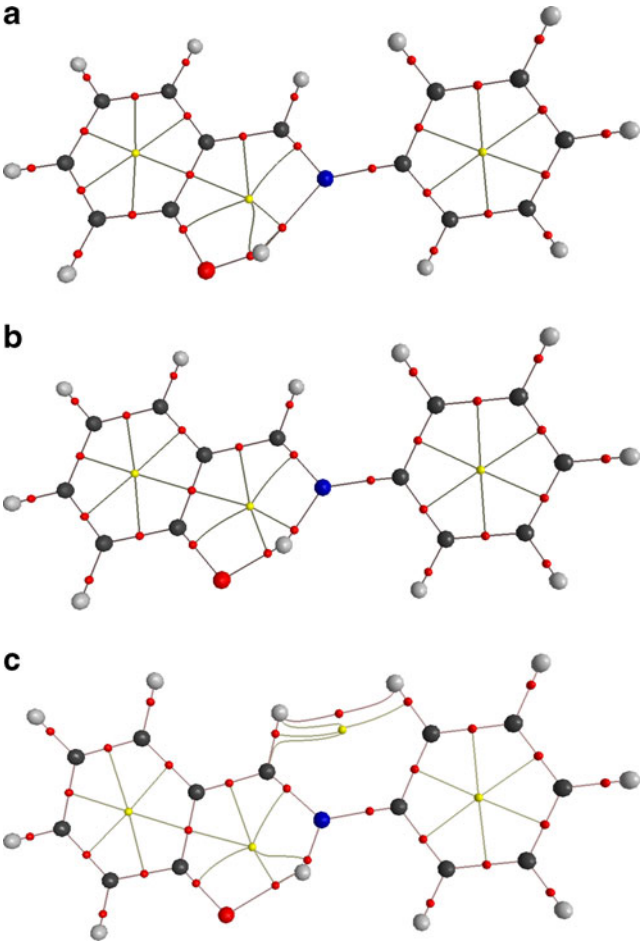

Fig. 3 Molecular graphs corresponding to the stable phenol (**a**), tautomeric transition state (**b**) and the stable NH (**c**) form of SA showing the positions and formations of all (3,–1) CPs (small red circles) and (3,+1) CPs (small yellow circles). (Color figure online)

between C7 and C9 from planarization of SA is stabilized by H-H bonding between H atoms attached to them. It can be stated that stabilization energy of H-H bonding in Fig. 3c is 4.65 kcal mol^{-1}. On the other hand, (3,+1) CP close to (3,–1) CP showing only presence of a H-H bonding between H7 and H9 in Fig. 3c cannot be regarded as a RCP, because two nuclear attractors contribute to the formation of that CP, which is of obvious incongruity with conventional definition of RCPs in ref. 17(c).

It is well-known that the heteroatom bonds are those most affected by molecular self-isomerization (intramolecular proton transfer). In this regard, C1—O and C7—N bonds are the most sensitive indicators of the structural form of the compound. The former is of single bond character in OH (phenol-imine or benzenoid) tautomers and of double bond character in canonical NH (*cis*-keto amine or quinoid) tautomers, while the latter is of double bond in OH (phenol-imine) tautomers and of single bond in canonical NH (*cis*-keto amine) tautomers as shown in Scheme 1. Monitoring the geometrical behaviors of them by PES, it is possible to observe certain characteristic changes in covalent topology of SA. It is inferred from the results in Fig. 4 that indicative bond lengths cannot reach their expected values even if tautomerization occurs in gas phase. At the seventeenth scan step equivalent to the stable NH tautomer, two of indicative bond lengths, O=C1 [1.261 Å] and C6=C7 [1.395 Å], are intermediate between the corresponding double (1.222 Å and 1.333 Å in benzoquinones) and single bonds (1.362 Å and 1.455 Å in phenols) [67], whereas C7—N bond length [1.331 Å] is close to its convenient value of 1.339 Å [67]. It is worth noting the changes in three of C—C bond lengths in salicylidene ring, C1—C2, C1—C6 and C5—C6 (Table 1). While C1—O and C7=N bonds become double and single bond as much as possible during the tautomerization respectively, single bond character of C1—C6 is more pronounced than that of C1—C2 and C5—C6 due to constructive resonance effects from the changes started in C1—O and C7=N bonds, proceeding in two different routes on the molecular skeleton. Geometrical examination of the changes in covalent topology of SA during proton transfer reaction shows that the stable NH form of SA can be regarded as a resonance hybrid of its zwitterionic and canonical *cis*-keto tautomer and bond lengths in the stable NH tautomer cannot reach their expected values even in gas phase.

Topological analysis for intramolecular charge transfer

Depending on proton transfer, not only do the most indicative heteroatom bonds vary, but also certain C—C bonds in salicylidene ring deviate from their optimal values (1.388 Å) as shown in Table 1. Therefore, to describe collective dynamics of the C—C bonds in salicylidene ring, we use PDI quantitatively indicating aromaticity of the ring.

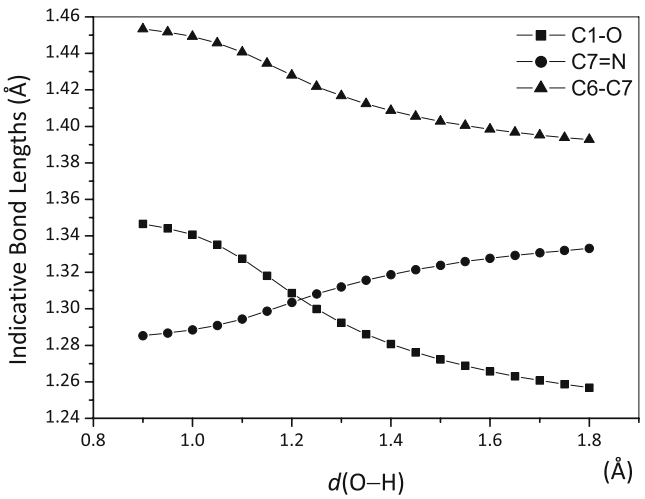

Fig. 4 Dependencies of the indicative bond lengths against the scan coordinate *d*(O—H)

Table 1 Some selected bond lengths for the stable OH and NH form of SA (Å) at B3LYP/6-311++G(d,p) level

Bond lengths	OH	NH	Bond Lengths	OH	NH
C1-C2	1.400	1.443	C8-C9	1.403	1.400
C2-C3	1.387	1.367	C9-C10	1.392	1.392
C3-C4	1.401	1.427	C10-C11	1.394	1.394
C4-C5	1.384	1.365	C11-C12	1.395	1.394
C5-C6	1.408	1.429	C12-C13	1.391	1.389
C6-C1	1.421	1.469	C13-C8	1.402	1.401
C1-O	1.341	1.261	C7-N	1.288	1.331
C6-C7	1.450	1.395	C8-N	1.409	1.406

PDI is a very useful tool to analyze the local aromaticity in different molecular fragments [43–47]. PDI for the salicylidene ring in the optimized ground state of SA is found as 0.083. This value is less than that of fully aromatic benzene (~0.100-0.103) [46, 47] due to π-electron donation from salicylidene ring to chelate ring. Throughout the proton transfer reaction total aromaticity of these adjacent moieties is approximately equal to that of fully aromatic benzene. Dependencies of PDI of salicylidene and chelate ring against hydroxyl bond elongation are shown in Fig. 5a and b. Aromaticity of salicylidene ring is continuously declined throughout the proton transfer reaction as shown in Fig. 5a. Similar results have been previously reported for SA derivatives by using another aromaticity indicator [14, 15]. As far as aromaticity behaviors of salicylidene and chelate ring (Fig. 5a and b) against hydroxyl bond elongation under the value of 1.50 Å of the scan coordinate are concerned that the loss in aromaticity of the former is compensated by augmentation in aromaticity of the latter. This behavior is convenient with the fact that SA in NH form is less stable by 4.65 kcal mol^{-1} due to the loss in aromaticities of salicylidene and chelate ring. For more distant values of the scan coordinate, concomitant decrease in aromaticities of both salicylidene and chelate ring is occurred by different extents. There is a dynamic balance between them against the tautomeric proton movement in SA. Reason for concomitant decrease in aromaticities of both fragments will be explained in the latter sections. During the proton transfer, PDI of aniline ring remains almost constant in a narrow interval, 0.0929–0.0943.

Electron density or its Laplacian at RCPs of the salicylidene and chelate ring have different characteristic, since the latter is established on a hydrogen bridge. While PDIs correlate well with electron density and its Laplacian at RCP of the salicylidene ring, this tendency is not observed for the chelate ring (see Fig. S1 in Electronic supplementary information file). Thus, it can be stated that $\rho(\mathbf{r}_{RCP})$ and $\nabla^2\rho(\mathbf{r}_{RCP})$ are useful parameters to describe changes in aromaticity for the ring system consisting of

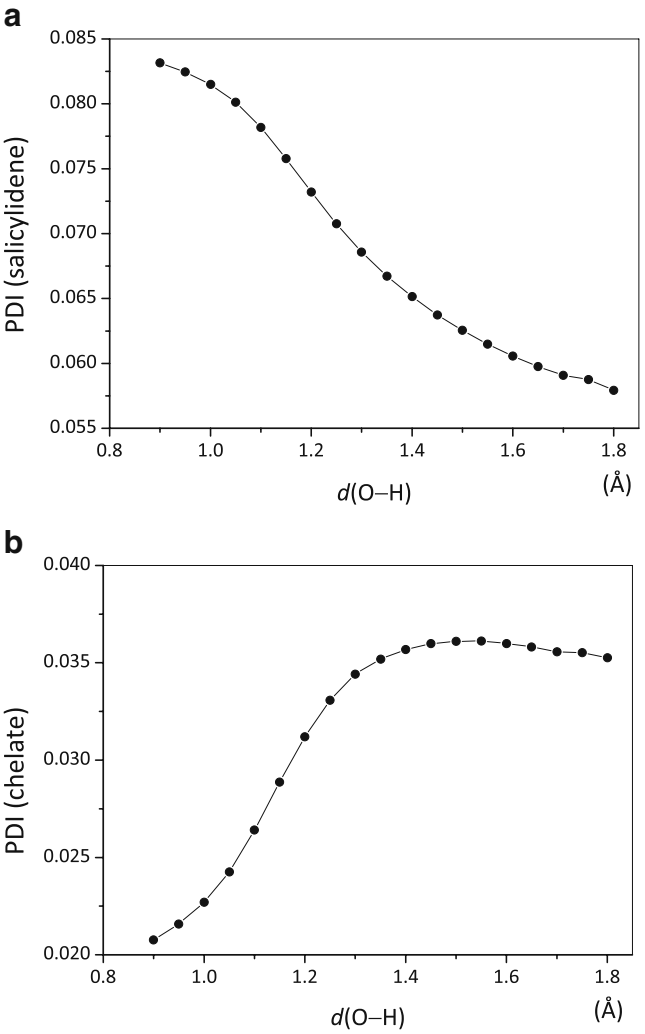

Fig. 5 Evolution of PDIs for salicylidene (**a**) and chelate ring (**b**) against hydroxyl bond elongation

purely covalent bonds, but not for quasiaromatic system such as chelate ring.

The interrelations of $\rho(\mathbf{r}_{BCP})$ values for hydroxyl (OH) and amine (NH) bond with their relevant bond lengths (Fig. 6a) show an exponential decay, whereas corresponding interrelations of C1—C6, C6—C7, C1—O and C7—N bonds in the chelate ring are linear (see Fig. S2 in Electronic supplementary information file). QTAIM methodology can be used to correlate the formal bond order with electron density at the BCP [53, 54] and electron density at BCP increases linearly as the bond length decreases [68]. According to Espinosa *et al.* [55], the presence of intramolecular H-bond in SA is responsible for this exponential behavior of hydroxyl and amine bond. It has been recently reported that similar inference is valid for the experimentally observed geometries of different *o*-hydroxy aryl Schiff base species [69]. The value of $\rho(\mathbf{r}_{BCP})$ can be seen as a measure of the bond order or

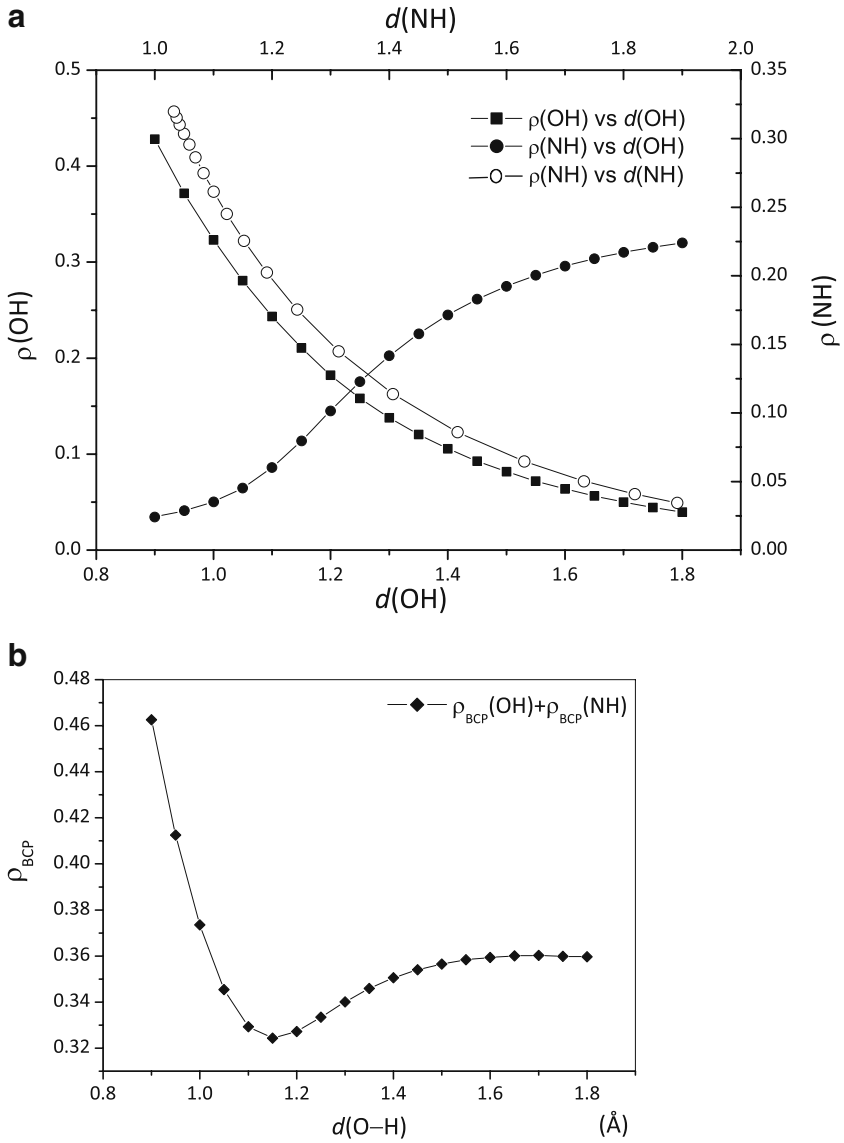

Fig. 6 (**a**) Variations of electron densities (in e/Å^3) at BCPs of hydroxyl (OH) and amine (NH) bonds against the related bond elongations. (**b**) Summation of electron densities at BCPs of hydroxyl and amine bonds against hydroxyl bond elongation

bond valence [53, 54]. While the relatively large and negative large values of $\rho(\mathbf{r}_{BCP})$ and $\nabla^2\rho(\mathbf{r}_{RCP})$ indicating electronic charge concentration along the relevant bond path are observed for the shared interactions (covalent bonds), they have low and positive low values indicating electronic charge depletion along the relevant bond path, which their formation mechanism are partial covalent character [70]. Therefore, these observations are reasonable, since zwitterionic form of SA plays an important role in the formation of intramolecular H-bond.

Relationship between bond order and electron density for intramolecular H-bond of SA

An elegant way to investigate heteronuclear H-bonds is based on the valence (or bond order) calculations [71], enabling a quantitative evaluation for the valence of tautomeric proton (v). Valence of protons in O—H···N and O···H—N type H-bonding is calculated by the following equation;

$$v = \exp\left(\frac{r_0 - r}{b}\right), \tag{6}$$

in valence units (v.u.), where b=0.371 for O—H and b= 0.385 for N—H, r stands for the distance between H and acceptor or donor atom, r_0 is equal to 0.942 for O—H and to 0.992 for N—H [71]. The rule of bond order conservation requires that the summation of the calculated v values for tautomeric proton ($v_{O—H}+v_{H\cdots N}=v_{O\cdots H}+v_{H—N}$) is formally equal to 1.00. Variation of valence of tautomeric proton in hydroxyl and amine bond and total bond valence of the tautomeric proton with hydroxyl bond elongation is shown in Fig. 7. As seen from Fig. 6a, dependencies of charge densities at BCPs in hydroxyl and amine bond against the

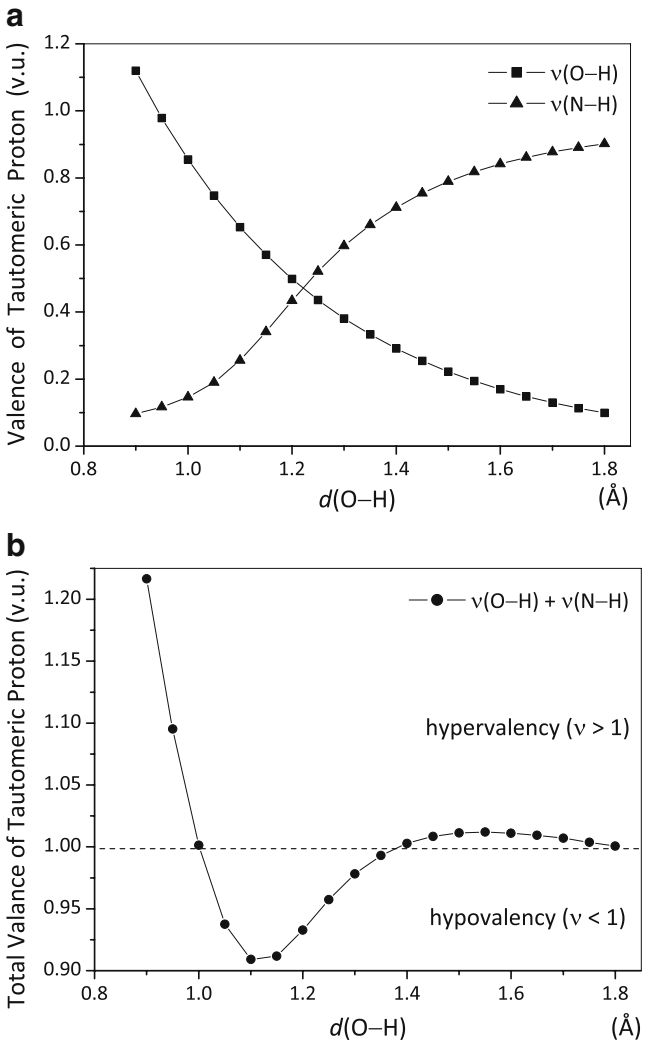

Fig. 7 Variation in the valences of tautomeric proton in hydroxyl and amine bonds (**a**) and the total valence of tautomeric proton (**b**) against hydroxyl bond elongation. Dashed line shows formal valence (or bond order, v=1) level of tautomeric proton

relevant bond lengths display the same behaviors with those of their valences in Fig. 7a.

According to the Fig. 7b, valence of the tautomeric proton has rapidly decreased by incipient proton transfer until it reaches to a minimum value (0.909) from relatively high initial valence value of 1.217, resulting in a transition from hypervalency (v>1) to hypovalency (v<1) region. It augments with the growing predominance of the NH form (superposition of canonical *cis*-keto and zwitterionic) to compensate deficiency in electronic population on the tautomeric proton and then, converges slightly over its formal value of 1.00 toward stable NH tautomer. Considering the valence of tautomeric proton of both the stable OH tautomer appeared in third step and stable NH tautomer appeared around seventeenth step, it can be stated that the stable tautomers are observed in the vicinity of formal valence of the tautomeric proton. Molecular structures corresponding to below this value can be regarded as tautomeric transition states (TSs), whereas tautomeric protons in stable OH and NH tautomers in crystal phase have a considerably higher value of 1.00. This inference is experimentally verified by H-bonds reported in [27, 30]. Valences of tautomeric proton located in vicinity of the midpoint of the hydrogen bridge are obtained as 0.829 and 0.905 with regard to geometric details of H-bonds in [27, 30], while those of other stable tautomeric forms in [27, 30] are higher than 1.00 in the interval of 1.015-1.214. Valence of the tautomeric proton in TSs is reduced to below its formal value of 1.00, indicating partial positive charge (+δ) on the tautomeric proton. This result is consistent with the H-bond in SA having partial electrostatic character suggested by the results from QTAIM analysis above. It is inferred from these results that overabundance in the valency of tautomeric proton of the initial OH form leads to proton transfer reaction and ultimately the tautomerization culminates in almost formal single valence of the tautomeric proton for both stable OH and NH form in gas phase.

QTAIM methodology forecasts the exponential relationship between formal bond order (v) and $\rho(\mathbf{r}_{BCP})$ values according to the following equation [53, 54]

$$v = \exp[A(\rho_{BCP} - B)], \tag{7}$$

where A and B are arbitrary constants with convenient units. In this regard, an intriguing result is obtained by examining this relation hydroxyl and amine bonds in the chelate ring. Contrary to the expected exponential behavior prescribed by Eq. 7, variations of bond orders involving tautomeric proton correlate linearly with the relevant electron density values at their BCPs as shown in Fig. 8. Since intramolecular H-bond in SA is partially covalent, it is seen that Eq. 7 ceases to be valid for the bonds which are not purely covalent. This inference is novel and of great importance for the relevant scientific community. Consequently, investigation of the relationship between bond orders and electron density value at BCP can inform about the formation character of a bond. If there is an exponential relationship between them as in Eq. 7, then one can straightforwardly say that the bond is purely covalent, whereas there is a linear relationship between them as shown in Fig. 8a and b then that bond is partially covalent.

Topological analysis regarding intramolecular H-bonding

The strength of intramolecular H-bond is straightforwardly described as a difference between the sum of the non-covalent van der Waals radii [62] of N and O atom (3.07 Å) and the interatomic separation from N to O atom during tautomeric proton migration, 3.07−d(O—N). This thought

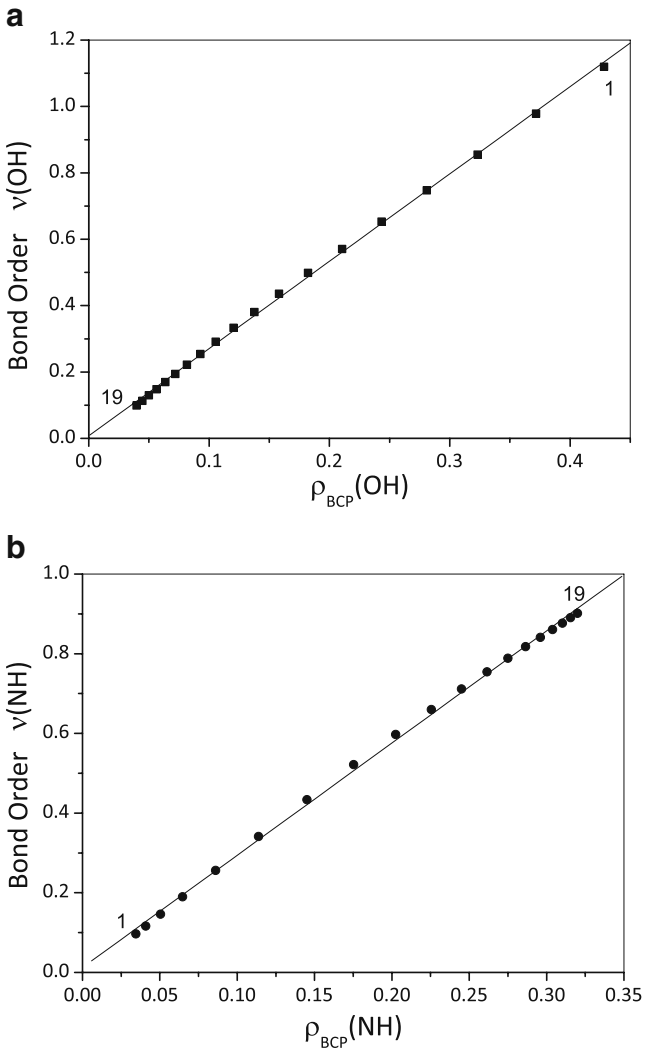

Fig. 8 Correlations between formal bond orders (v) and electron density values (in e/Å^3) at BCP of hydroxyl and amine bonds: (**a**) $v(OH)=2.6307\rho_{BCP}(OH)+0.00739$, $R^2=0.9996$ (**b**) $v(NH)=2.81679\rho_{BCP}(NH)+0.01248$, $R^2=0.99945$. Only the first and last steps are named and the other points between them are arrayed respectively in their associated line

is a prevalently acceptable and means that the shorter hydrogen bridge the stronger H-bond. Variation of the strength of intramolecular H-bond throughout the scan process is shown in Fig. 9a. According to Fig. 9a, intramolecular H-bonds in tautomeric TSs (O···H···N) of SA is stronger than those o O—H···N or O···H—N tautomeric forms of SA. It is in agreement with the Leffler–Hammond rule [72, 73], expressing that the systems closer to TSs the stronger H-bonds than those species far from TSs. This result is experimentally confirmed by Filarowski *et al.* for distinct *o*-hydroxy aryl Schiff base species in refs. [27, 28, 30, 69] and computationally proposed in refs. [14, 15] for different SA derivatives. The interrelation between δ(O,N) and *d*(O—N) reveals that the shortening in the distance between the heteroatoms increases the delocalization index between them as shown in Fig. 9b and vice versa. In addition, similar linear correlations against *d*(O—N) are obtained for electron density (Fig. S3a) and its Laplacian (Fig. S3b) at RCP of chelate ring. Since the reduction of the *d*(O—N) implies the strengthening of the intramolecular H-bond, topological parameters electron density (ρ and $\nabla^2\rho$) at RCP of the chelate ring can be regarded as alternative indicators for the strength of intramolecular H-bond as reported in [19–24]. According to the results presented here, delocalization index δ(O,N) indicating the amount of sharing electrons between donor and acceptor atom of heteronuclear H-bond is also another useful descriptor for the strength of H-bond due to the fact that the shortening of the distance between O and N results in the augmentation of the amount of sharing electrons between donor and acceptor atom as shown in Fig. 9b. This fact is verified by the correlation between geometric criterion for the strength of H-bond $3.07-d$(O—N) and its topological counterpart δ(O,N) as shown in Fig. 9b. Considering only the distances between the donor and acceptor atom, it can be stated that intramolecular H-bonds in SA can be regarded as low barrier hydrogen bonds (LBHB), since the corresponding distances between donor and acceptor atom of O—H···N (or O···H—N) type LBHBs are less than 2.65 Å [27]. This is in agreement with the fact that the potential barrier height (6.29 kcal mol^{-1}) is sufficiently small.

Figure 9c showing scatter plot of H-bond strength against average delocalization index within chelate ring can be seen as a direct evidence for resonance assisted character of intramolecular H-bond in SA. RAHB model [74, 75] states that π-electron delocalization results in enhancement of H-bond strength as shown in Fig. 9c. Linear correlation in Fig. 9c displays that the strength of H-bond increases with increasing aromaticity or π-delocalization level of chelate ring and vice versa. Thus, it can be mentioned that there is an electron transfer from the proton-donating O to the proton acceptor N, since hydroxyl group becomes a strong π-donor by incipient proton transfer in *o*-hydroxy Schiff bases [76].

Some authors [77–79] have reported that the direction of lone-pair electrons on N strongly influences the strength of intramolecular H-bond in Schiff bases. As far as Fig. 9d is concerned that LP electronic population on N also affects the strength of H-bond. It is worth noting that the strength of H-bond asymmetrically varies with hydroxyl bond elongation as shown in Fig. 9a due to heteronuclear nature of the intramolecular H-bond. Nonequivalent effects of O and N atom on proton transfer in the quasiaromatic chelate ring result in different behaviors of the strength of H-bond against the relevant electron density values at BCPs of hydroxyl and amine bond shown in Fig. S3c. Similar tendencies are observed in *o*-hydroxy aryl Schiff bases [69].

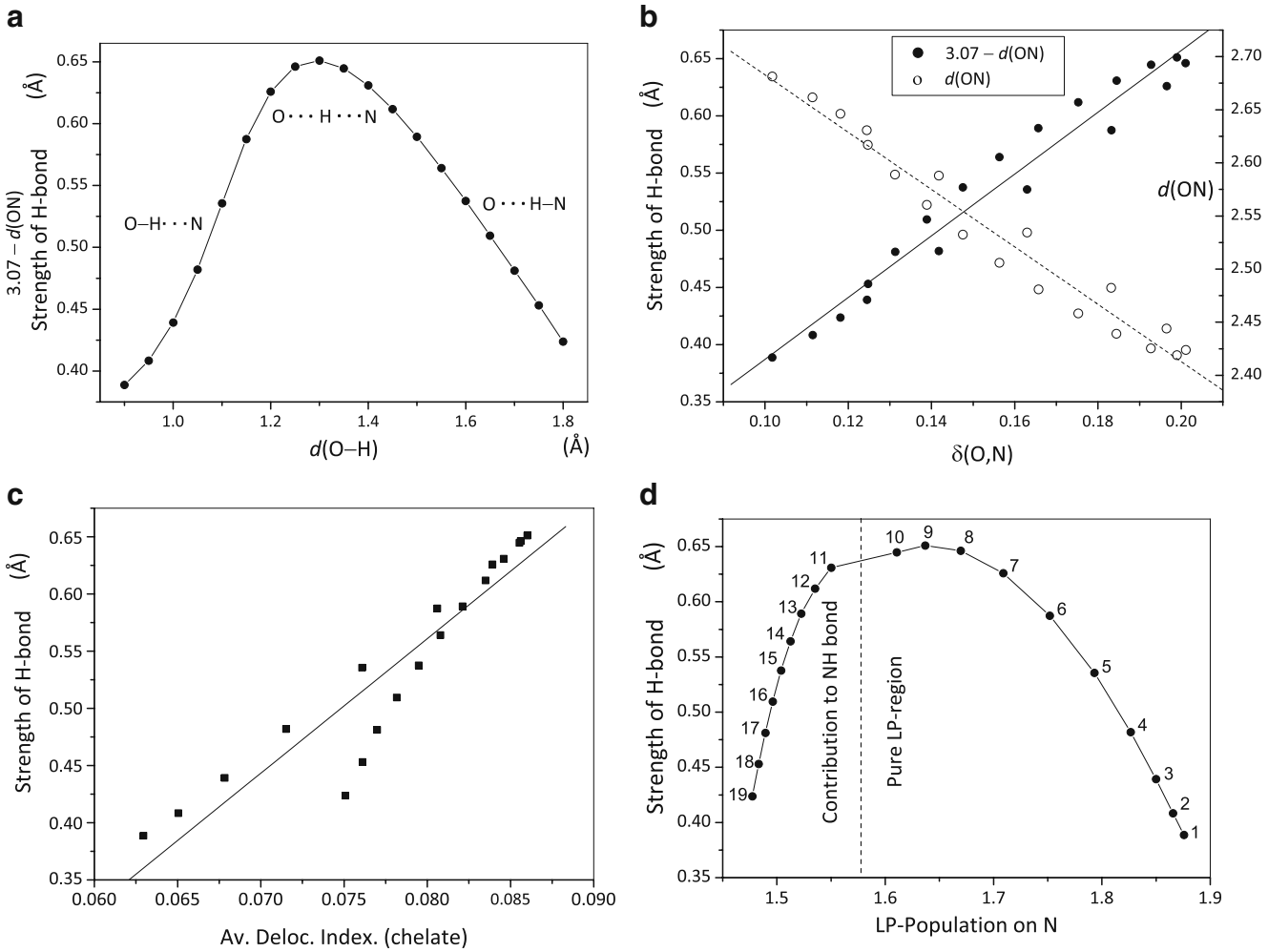

Fig. 9 (**a**) Strength of intramolecular H-bond against hydroxyl bond elongation; (**b**) Strength of H-bond (left vertical axis) and interatomic distance (right vertical axis) from N to O against variation of delocalization indices between O and N δ(O,N); (**c**) Scatter plot of the strength of H-bond against PDIs of chelate ring; (**d**) Interdependency between the Strength of H-bond and LP population on N with the corresponding step numbers. Linear correlations are expressed as; (**b**) Strength of H-bond =2.69927δ(O,N)+0.11729, R^2=0.98053 by solid line and *d*(O—N)=−2.69924δ(O,N)+2.95271, R^2=−0.98053 by dashed line; (**c**) Strength of H-bond =11.76778 Av. Deloc. Index (chelate) −0.38046, R^2=0.93266

Energetic aspects for intramolecular H-bonds in SA

The scatter plot of hydrogen bond dissociation energy (E_{HB}) prescribed by Espinosa *et al.* [56] against its strength is shown in Fig. 10a. Hydrogen bond energy of stable OH (third step) of SA is almost the same as that of NH (seventeenth step) form of SA, whereas their strengths are quite different. The respective values of them are found as 14.615 and 14.825 kcal mol^{-1}. These values are close to those of *o*-hydroxyaryl Schiff bases [69]. According to Fig. 10a, the strength of H-bond increases with increasing H-bond dissociation energy. The similar tendency can be obtained by using Musin & Mariam H-bond dissociation energy in Eq. 5 [57] as shown in Fig. 10b. H-bond dissociation energies calculated by using Eq. 5 for stable OH and NH form of SA are 10.898 and 12.953 kcal mol^{-1}, respectively. Considering correlation coefficients of Fig. 10a and b, it can be stated that Musin & Mariam's treatment for H-bond dissociation energy is more reliably than that of the approach by Espinosa *et al*. Of these, the former has been designed for intramolecular H-bond, whereas the latter has been developed for intermolecular H-bonds and overestimates the intramolecular H-bond dissociation energy for SA. Both approaches also agree with each other concerning the observation that TSs in tautomerism of SA have the strongest H-bonds with high dissociation energies.

Quantitative classification of H-bond of SA

Topological parameters of the BCPs intramolecular H-bond in SA are listed in Table 2. As mentioned before, positive Laplacian values of electron density at BCP usually indicate

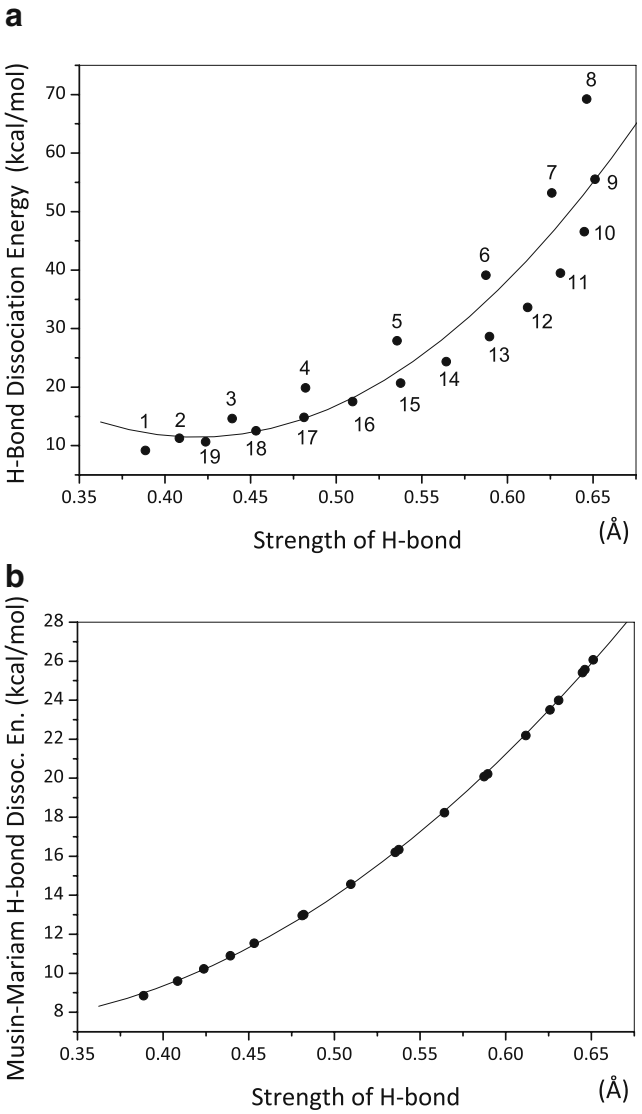

Fig. 10 Scatter plot of hydrogen bond dissociation energy E_{HB} estimated by $-V_C(\mathbf{r}_{BCP})/2$ (**a**) and Musin & Mariam H-bond dissociation energy (**b**) against its strength (X in Å). Correlations are expressed by (**a**) E_{HB} $(-V_C/2)=154.36529-682.43974\ X+814.66992\ X^2$, $R^2=0.88408$; (**b**) E_{HB} (Musin-Mariam) $=17.75337-74.66409\ X+134.09828\ X^2$, $R^2=0.99984$

the bonds by partially covalent interactions. Negative Laplacian values at BCPs between hydrogen and acceptor atom correspond to TSs in the seventh and eighth row in Table 2. Total electron energy density (H_C) as well as Laplacian of electron density ($\nabla^2\rho_C$) at BCP of H···A bond path are useful parameters to describe H-bond strength [80]. While both H_C and $\nabla^2\rho_C$ are positive for weak or medium H-bonds, both are negative for very strong H-bonds, for strong H-bonds $H_C<0$ and Laplacian $\nabla^2\rho_C>0$. All of total electron energy densities at BCPs of H···A bond paths are negative and most of Laplacian values except for TSs are positive. These two topological parameters are indicators for not only H bond strength but also its formation character [81, 82]. The interactions with positive Laplacian of the electron density and negative H_C are at least partially covalent in nature [81]. The negative and positive values of the $\nabla^2\rho_C$ reveal concentration and depletion of electronic charge density between the pair of interacting atoms corresponding to covalent bond and partially covalent interactions, respectively [82]. The results in Table 2 suggest that intramolecular H-bonds in tautomeric ensemble of SA are predominantly partial covalent in nature and the most strength H-bonds are observed for molecular entities close to TS. In addition, it is seen that the kinds of interactions can be connected to their strengths. From topological point of view, formation character of intramolecular H-bond is quantitatively analyzed by taking into account its $-V_C/G_C$ ratio between hydrogen and acceptor atom. This ratio is greater than 2 for covalent H-bonds, less than 1 for non-covalent H-bonds and between 1 and 2 for partially covalent H-bonds [83]. Variation of $-V_C/G_C$ ratio against H···A distances in the tautomeric ensemble of SA is shown in Fig. 11. According to Fig. 11, covalent character of H-bonds in TSs due to negative Laplacian is more pronounced than those of the other molecular entities in the tautomeric ensemble. Since topological parameters is blind to the kind of orbitals in which electrons are transferred and considers only the amount of the electron density between interacting atomic basins, we need further information about the kind of bonding orbitals leading to intramolecular H-bond of SA. At this point, NBO analyses may provide new insights in our discussion.

Complementary remarks from NBO analysis

Population changes in certain natural bond orbitals during the proton transfer are of fundamental importance in understanding electronic nature of tautomerism in SA and provide useful complementary remarks. Changes in population of LP orbital on N is shown in Fig. 12a. The exclusion of LP electrons on N makes the nitrogen a basic center in SA and facilitates to undergo a protonation at the nitrogen center. LP orbital on N is disappeared beyond the tenth step of the scan process due to the formation of NH bond with the aid of non-Lewis type valence orbital (LP*) on the tautomeric proton. Population of LP* orbital on the tautomeric proton reaches its maximum value for the molecular entities nearby TS as shown in Fig. 12b. LP* population on H is diminished by incipient proton transfer reaction and the stable OH form (at the third step) of SA has minimum LP* population. This observation is an astonishing result, because π-electron transfer electron transfer is occurred through formally unoccupied valence nonbonding LP* orbital on the tautomeric proton. After the formation of NH bond at the 11th step, LP* population is rapidly increased as shown in Fig. 12b. Another important result from NBO analyses is that LP* population for the stable OH form of SA is almost the same as that of stable NH form. The fact that intramolecular π-electron transfer accom-

Table 2 Topological parameters (in a.u.) of D—H and H···A BCPs. First eight rows for O—H···N and the others for N—H···O type H-bonds. The rows correspond to the considered steps in intramolecular proton transfer process, respectively

Step	D—H (BCP)					H···A (BCP)				
No	ρ_C	$\nabla^2\rho_C$	G_C	V_C	H_C	ρ_C	$\nabla^2\rho_C$	G_C	V_C	H_C
1	0.428	−3.349	0.086	−1.009	−0.923	0.035	0.109	0.028	−0.029	−0.001
2	0.372	−2.733	0.074	−0.832	−0.758	0.041	0.112	0.032	−0.036	−0.004
3	0.323	−2.203	0.068	−0.687	−0.619	0.050	0.111	0.037	−0.047	−0.009
4	0.281	−1.674	0.067	−0.553	−0.486	0.065	0.101	0.044	−0.063	−0.019
5	0.243	−1.158	0.071	−0.432	−0.361	0.086	0.072	0.054	−0.089	−0.036
6	0.211	−0.712	0.079	−0.336	−0.257	0.114	0.002	0.063	−0.125	−0.062
7	0.182	−0.372	0.086	−0.265	−0.179	0.145	−0.133	0.068	−0.170	−0.101
8	0.158	−0.140	0.090	−0.214	−0.125	0.175	−0.328	0.069	−0.221	−0.151
9	0.202	−0.550	0.068	−0.273	−0.205	0.138	0.004	0.089	−0.177	−0.088
10	0.226	−0.772	0.065	−0.322	−0.257	0.120	0.087	0.085	−0.149	−0.063
11	0.245	−0.973	0.061	−0.365	−0.304	0.106	0.131	0.079	−0.126	−0.047
12	0.261	−1.147	0.058	−0.402	−0.344	0.093	0.151	0.073	−0.107	−0.035
13	0.275	−1.292	0.055	−0.432	−0.378	0.082	0.159	0.066	−0.091	−0.026
14	0.286	−1.410	0.052	−0.457	−0.405	0.072	0.160	0.059	−0.078	−0.019
15	0.296	−1.504	0.050	−0.477	−0.427	0.064	0.157	0.053	−0.066	−0.013
16	0.304	−1.579	0.049	−0.493	−0.444	0.056	0.152	0.047	−0.056	−0.009
17	0.310	−1.637	0.048	−0.505	−0.457	0.050	0.145	0.042	−0.047	−0.006
18	0.316	−1.678	0.047	−0.514	−0.467	0.045	0.136	0.037	−0.040	−0.003
19	0.320	−1.712	0.047	−0.521	−0.475	0.040	0.127	0.033	−0.034	−0.001

panying proton transfer in SA comes into being through formally vacant LP* orbitals on the tautomeric proton is not contradictory for classifying intramolecular H-bonds of SA as covalent or partially covalent, because the formation of a covalent bond does not necessarily bring about electronic charge condensation in the bonding orbitals [81].

Appearance of negative Laplacian values for H···A bonds arises from a considerable augmentation in the amount of electronic charge through low-lying formally vacant π-type LP* orbitals on the tautomeric proton. The formation of zwitterionic form of SA as a result of the strain of initial intramolecular H-bond by hydroxyl bond elongation can be regarded as a physical basis for partially covalent nature of hydrogen bridge. The linear correlations between the orders of hydroxyl (or amine) bond and the relevant electron density values at BCPs in Fig. 8 prove evidently that intramolecular H-bonds are essentially formed by partial covalent interactions. It is worth noting that the covalent character of D—H bonds is decreased with increasing covalent character of H···A bonds as shown in Table 2. This case can be understood by the presence of electronic charge transfer in hydrogen bridge from the former to latter. The low-lying formally vacant *p*-type LP* orbitals of $H^{+\delta}$ cation mediate this charge transfer. The mentioned charge transfer is not restricted within the hydrogen bridge. Moreover, aromaticity balance between salicylidene and chelate ring can be regarded as a driving force in background of the intramolecular charge transfer.

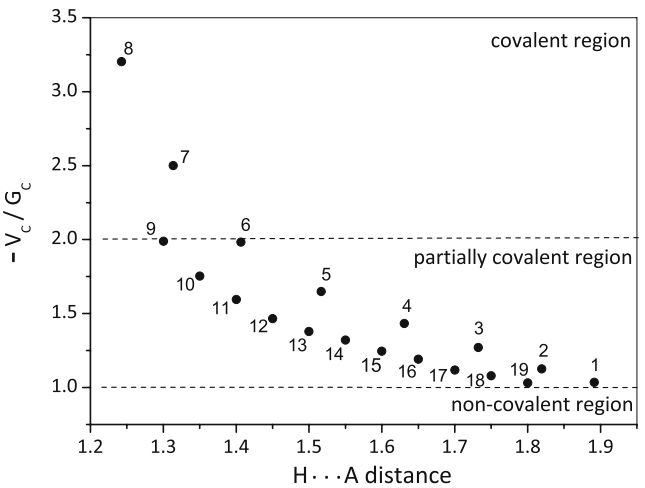

Fig. 11 Scatter plot of $-V_C/G_C$ ratio against H···A distances of intramolecular H bonds in the tautomeric ensemble of SA with the corresponding step numbers

After the formation of NH bond, electronic contribution from N to NH bond continues to decrease as shown in Fig. 12a. This diminishment is accompanied with decrease in aromaticity level of salicylidene ring shown in Fig. 12c. It is inferred from these results that LP orbital on N center together with salicylidene ring donate electronic charge to the formation of π-delocalized system in the chelate ring. This additional electron donation from LP orbital on N beyond the third step in proton movement suggest that quasiaromatic chelate ring formation is established not only to compel a reduced aromaticity of salicylidene ring but also to decrease in electronic population on N. As mentioned

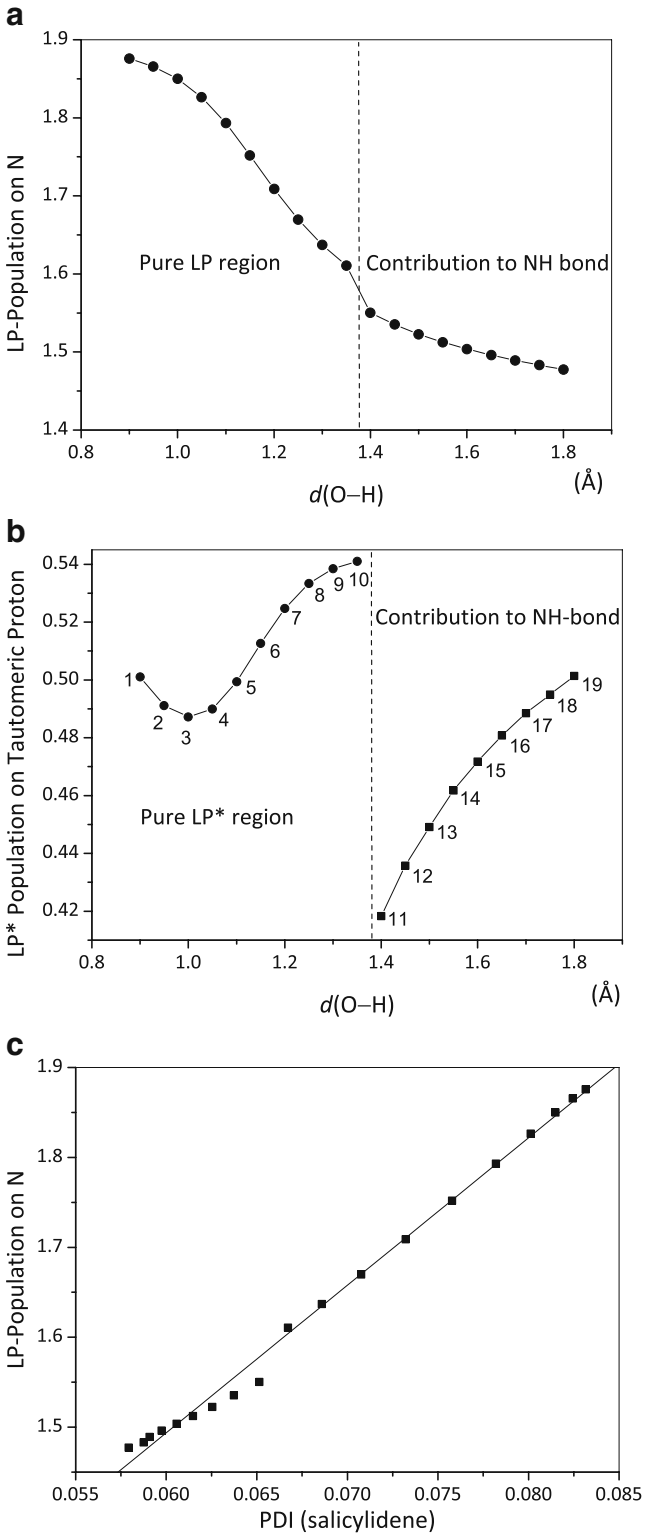

Fig. 12 Variation in LP-Population on N (**a**) and LP*-Population on the tautomeric proton (**b**) against hydroxyl bond elongation. Vertical dashed lines separate pure LP on N (or LP* on H) region from the contribution to NH bond of LP orbital on N (or LP* orbital on H). Interrelation between LP-Population on N (y) and PDI of salicylidene ring (x) with the corresponding step numbers (**c**). Linear correlation is expressed by y=16.40771 ×+0.50922, R^2=0.99741

before, according to Filarowski *et al.* [27–30], quasiaromatic chelate ring formation has arisen from only decreasing in aromaticity of salicylidene ring; whereas the results presented in this study suggest that the formation of the chelate ring cannot be explained having regard to only decreasing in aromaticity of salicylidene ring. This complementary result is an advantage of tautomeric ensemble approach.

Concomitant decrease in aromaticities of salicylidene and chelate ring

Positive curvature of the electron density $\lambda_3(\mathbf{r}_{BCP})$ can be regarded as a measure of the overlap between the electron clouds of the atoms at the edges of the relevant bond path [54]. Dependencies of $\lambda_3(\mathbf{r}_{BCP})$ of hydroxyl and amine bond against corresponding electron density values at BCPs are

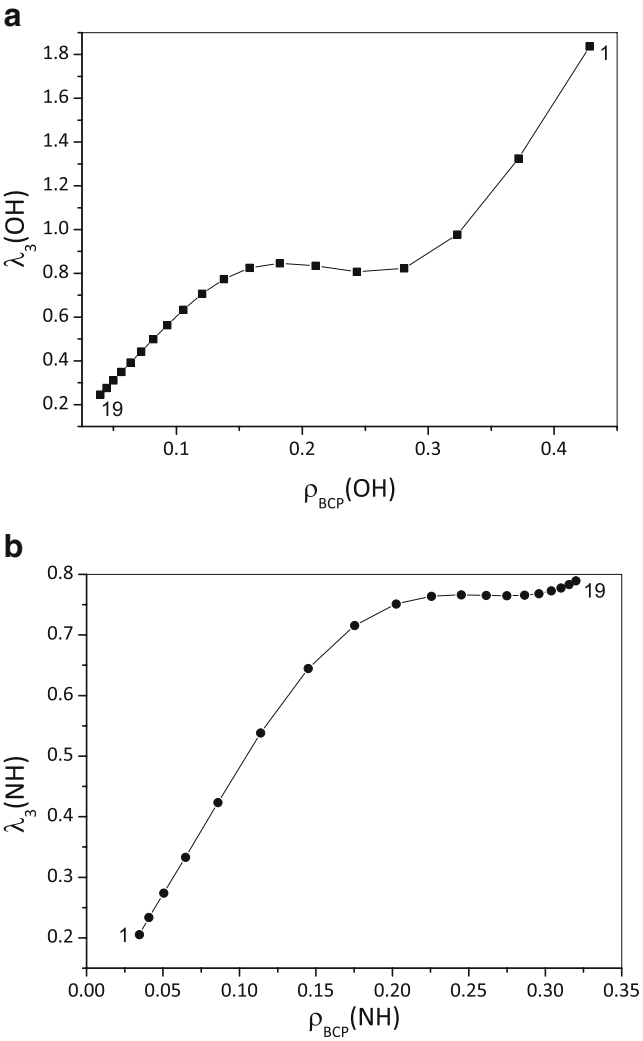

Fig. 13 Positive curvatures of the electron density of the hydroxyl and amine bond against electron density value at the relevant BCPs. Only the first and last steps are named and the other points between them are arrayed respectively in the associated curve for the sake of clarity

shown in Fig. 13. There is a plateau between the stable OH form (appeared at the third step) and TS (appeared at the ninth step) for the hydroxyl bond as shown in Fig. 13a. δ(O, N) indicating the amount of the shared electrons between O and N is considerably increased in the plateau according to Fig. 9b. Beyond this plateau, electron clouds on O and H are rapidly separated from each other. This fact reflects the growing predominance of the NH form regarded as resonance hybrid of canonical *cis*-keto and zwitterionic form. Thus, π-electron transfer from salicylidene to chelate ring is prevented beyond tautomeric TS appeared at the ninth step as shown in Fig. 5b. In addition, charge donation from N to the formation of amine bond is also decreased after the ninth step as shown in Fig. 12a. As a result of these tendencies, aromaticity of the chelate ring is somewhat decreased concurrently with that of salicylidene as shown in Fig. 5a and b. Another important characteristic for the plateau is deficiency in valence of the tautomeric proton indicating partial positive charge on it (Fig. 7b). On the other hand, $\lambda_3(\mathbf{r}_{BCP})$ of NH displays a different behavior as shown in Fig. 13b. Overlap between the electron clouds on N and H is rapidly increased by incipient proton transfer reaction up to the saturation observed in transition state region. Predominance of NH forms in the tautomeric equilibrium of SA is responsible for this saturation in the overlap between electron clouds of the tautomeric proton and nitrogen atom. The plateau region in Fig. 13a corresponds to considerable augmentation in π-electron transfer from salicylidene to chelate ring, while saturation region in Fig. 13b characterizes to the concomitant decrease in aromaticities of both adjacent fragment.

Concluding remarks

The purpose of this study is to describe properly the effects from intramolecular proton transfer reaction on the electronic properties and aromaticities of certain fragments in SA monitoring by a relaxed PES scan. Tautomeric proton is easily transferred to imine bridge because the activation energy is sufficiently small (6.29 kcal mol^{-1}). During tautomeric proton movement, SA becomes planar and geometrical parameters such as bond lengths cannot reach their expected values in canonical *cis*-keto form even if the tautomerization occurrs in gas-phase. Covalent skeleton of the stable NH form corresponds to a resonance hybrid of canonical *cis*-keto and zwitterionic form. Thus, π-electron delocalization is a driving force which is responsible for these geometric changes. NH tautomeric form is less stable than OH form by 4.65 kcal mol^{-1}. The enhanced quasiaromaticity within chelate ring stabilizes NH tautomer.

The results have pointed out that π-electron transfer mechanism in SA is of importance in understanding of chemical background underlying its tautomerism. The use of *tautomeric ensemble* approach in examination of aromaticity balance reveals that electron deficiency in LP orbital on N facilitates to the protonation at N-center and to chelate ring formation. Quasiaromatic chelate ring is established not only to compel a reduced aromaticity of salicylidene ring but also to decrease in LP-population on N. These results unequivocally suggest that aromaticity balance between salicylidene and chelate ring results in the greater π-electron delocalization within pseudo-ring for molecular entities regarded as TS in tautomeric ensemble what leads also to strengthening of the intramolecular H-bonding. Intramolecular H-bond in SA is classified as RAHB which influences the electronic states of its neighboring aromatic fragments. This feature may offer an opportunity for their usage in synthesis of versatile charge transfer complexes possessing valence tautomerism and metalloaromaticity property [84–86].

Topological analysis on the tautomeric ensemble of SA suggests that intramolecular H-bonds in SA are predominantly arisen from partially covalent interactions as shown in Fig. 11, emphasizing significance of the zwitterionic form in the tautomeric equilibrium of SA. The amount of electron population in LP* orbitals on the tautomeric proton is increasingly augmented toward tautomeric transition state as shown in Fig. 12b. As a result of this, the tautomeric proton has become hypovalent. In addition, hypervalent character of the tautomeric proton is responsible for incipient proton transfer reaction. Hypovalent character of the tautomeric proton in TSs is in agreement with the fact that non-Lewis LP* orbital on the tautomeric proton mediates electronic charge transfer through π-delocalized systems of the adjacent fragments, salicylidene and chelate ring. In methodological sense, the most important finding in the present study is that orders of hydroxyl (OH) and amine (NH) bond correlate linearly with their corresponding electron density values at the relevant BCPs (Fig. 8) due to partial covalent character of intramolecular H-bond. This result has not been reported in the literature yet.

Acknowledgments This study was supported by the Dokuz Eylül University Research Fund (grant 2007.KB.FEN.36). R.S. thanks TÜBİTAK (The Scientific and Technical Research Council of Turkey) for partial financial support.

References

1. Wang Y, DuBois JL, Hedman B, Hodgson KO, Stack TDP (1998) Science 279:537–540
2. Atwood DA, Harvey MJ (2001) Chem Rev 101:37–52
3. Hoshino N (1998) Coord Chem Rev 174:77–108
4. Vigato PA, Tamburini S (2004) Coord Chem Rev 248:1717–2128
5. Ortiz-Sanchez JM, Gelabert R, Moreno M, Lluch JM (2006) J Phys Chem A 110:4649–4656
6. Fabian WMF, Antonov L, Nedeltcheva D, Kamounah FS, Taylor PJ (2004) J Phys Chem A 108:7603–7612

7. Cohen MD, Schmidt GMJ (1962) J Phys Chem 66:2442–2446
8. Cohen MD, Schmidt GMJ, Flavian S (1964) J Chem Soc 2041-2051
9. Amimoto K, Kawato T (2005) J Photochem Photobiol C 6:207–226
10. Hadjoudis EM, Mavridis I (2004) Chem Soc Rev 33:579–588
11. Karabiyik H, Guzel B, Aygun M, Boga G, Buyukgungor O (2007) Acta Crystallogr C 63:o215–o218
12. Karabiyik H, Ocak-Iskeleli N, Petek H, Albayrak C, Agar E (2008) J Mol Struct 873:130–136
13. Petek H, Albayrak C, Odabasoglu M, Senel I, Buyukgungor O (2008) J Chem Crystallogr 38:901–905
14. Karabiyik H, Petek H, Iskeleli NO, Albayrak C (2009) Struct Chem 20:1055–1065
15. Petek H, Albayrak C, Odabasoglu M, Senel I, Buyukgungor O (2010) Struct Chem 21:681–690
16. The systematic name for salicylideneaniline (SA) is (*E*)-2-phenyliminomethyl phenol Its alternative names are 2-hydroxybenzylideneaniline or phenylsalicylaldimine
17. Dominiak PM, Grech E, Barr G, Teat S, Mallinson P, Wozniak K (2003) Chem Eur J 9:963–970
18. Krygowski TM, Wozniak K, Anulewicz R, Pawlak D, Kolodziejski W, Grech E, Szady A (1997) J Phys Chem A 101:9399–9404
19. Grabowski SJ (2001) J Mol Struct 562:137–143
20. Grabowski SJ (2002) Monatsh Chem 133:1373–1380
21. Grabowski SJ (2003) J Phys Org Chem 16:797–802
22. Grabowski SJ (2007) J Mol Struct THEOCHEM 811:61–67
23. Sobczyk L, Grabowski SJ, Krygowski TM (2005) Chem Rev 105:3513–3560
24. Palusiak M, Krygowski TM (2007) Chem Eur J 13:7996–8006
25. Dziembowska T, Rozwadowski Z (2001) Curr Org Chem 5:289–313
26. Filarowski A, Koll A, Glowiak T (2002) J Mol Struct 615:97–108
27. Filarowski A, Koll A, Glowiak T (2002) J Chem Soc, Perkin Trans 2:835–842
28. Filarowski A (2005) J Phys Org Chem 18:686–698
29. Filarowski A, Kochel A, Cieslik K, Koll A (2005) J Phys Org Chem 18:986–993
30. Filarowski A, Kochel A, Kluba M, Kamounah FS (2008) J Phys Org Chem 21:939–944
31. Peng C, Ayala PY, Schlegel HB, Frisch MJ (1996) J Comput Chem 17:49–56
32. Schlegel HB (1982) J Comput Chem 3:214–218
33. Hertwig RH, Koch W (1997) Chem Phys Lett 268:345–351
34. Becke AD (1988) Phys Rev A 38:3098–3100
35. Lee C, Yang W, Parr RG (1988) Phys Rev B 37:785–789
36. Klene M, Li X, Knox JE, Hratchian HP, Cross JB, Adamo C, Jaramillo J, Gomperts R, Stratmann RE, Yazyev O, Austin AJ, Cammi R, Pomelli C, Ochterski JW, Ayala PY, Morokuma K, Voth GA, Salvador P, Dannenberg JJ, Zakrzewski VG, Dapprich S, Daniels AD, Strain MC, Farkas O, Malick DK, Rabuck AD, Raghavachari K, Foresman JB, Ortiz JV, Cui Q, Baboul AG, Clifford S, Cioslowski J, Stefanov BB, Liu G, Liashenko A, Piskorz P, Komaromi I, Martin RL, Fox DJ, Keith T, Al-Laham MA, Peng CY, Nanayakkara A, Challacombe M, Gill PMW, Johnson B, Chen W, Wong MW, Gonzalez C, Pople JA (2004) Gaussian 03, Revision C02. Gaussian Inc, Wallingford
37. Foster JP, Weinhold F (1980) J Am Chem Soc 102:7211–7218
38. Reed AE, Weinhold F (1983) J Chem Phys 78:4066–4073
39. Reed AE, Weinstock RB, Weinhold F (1985) J Chem Phys 83:735–746
40. Bader RFW (1985) Acc Chem Res 18:9–15
41. Bader RFW (1991) Chem Rev 91:893–928
42. Bader RFW (1994) Atoms. In Molecules: a quantum theory. Oxford University Press, Oxford
43. Poater J, Duran M, Solà M, Silvi B (2005) Chem Rev 105:3911–3947
44. Merino G, Vela A, Heine T (2005) Chem Rev 105:3812–3841
45. Mandado M, Gonzalez-Moa MJ, Mosquera RA (2007) J Comput Chem 28:127–136
46. Poater J, Fradera X, Duran M, Solà M (2003) Chem Eur J 9:400–406
47. Fradera X, Austen MA, Bader RFW (1999) J Phys Chem A 103:304–314
48. Krygowski TM, Cyranski MK (2004) Phys Chem Chem Phys 6:249–255
49. Bultinck P, Rafat M, Ponec R, van Gheluwe B, Carbo-Dorca R, Popelier P (2006) J Phys Chem A 110:7642–7648
50. Poater J, Solà M, Duran M, Fradera X (2002) Theor Chem Acc 107:362–371
51. AIM2000 designed by Friedrich Biegler-König, University of Applied Sciences, Bielefeld, Germany
52. Firme CL, Antunes OAC, Esteves PM (2009) Chem Phys Lett 468:129–133
53. Bader RFW, Slee TS, Cremer D, Kraka E (1983) J Am Chem Soc 105:5061–5068
54. Espinosa E, Souhassou M, Lachekar H, Lecomte C (1999) Acta Crystallogr B 55:563–572, and references therein
55. Bader RFW, Preston HJT (1969) Int J Quantum Chem 3:327–347
56. Espinosa E, Molins E, Lecomte C (1998) Chem Phys Lett 285:170–173
57. Musin RN, Mariam YH (2006) J Phys Org Chem 19:425–444
58. Ogawa K, Fujiwara T (1999) Chem Lett 7:657–658
59. Popovic Z, Pavlovic G, Roje YH, Doslic N, Matkovic-Calogovic D, Leban I (2004) Struct Chem 15:587–598
60. Marston CC, Balint-Kurti G (1989) J Chem Phys 91:3571–3576
61. Popelier PLA (2000) Coord Chem Rev 197:169–189
62. Bondi A (1964) J Phys Chem 68:441–451
63. Matta CF, Hernandez-Trujillo J, Tang T-H, Bader RFW (2003) Chem Eur J 9:1940–1951
64. Poater J, Solà M, Bickelhaupt FM (2006) Chem Eur J 12:2889–2895
65. Poater J, Solà M, Bickelhaupt FM (2006) Chem Eur J 12:2902–2905
66. Bader RFW (2006) Chem Eur J 12:2896–2901
67. Allen FH, Watson DG, Brammer L, Orpen AG, Taylor R (2004) In: Prince E (ed) International tables for crystallography (Vol C): mathematical, physical and chemical tables, 3rd edn. Kluver, Dordrecht, pp 790–811
68. Bader RFW, Tang TH, Tal Y, Biegler-König FW (1982) J Am Chem Soc 104:946–952
69. Filarowski A, Majerz I (2008) J Phys Chem A 112:3119–3126
70. Koritsanszky TS, Coppens P (2001) Chem Rev 101:1583–1627
71. Steiner T (1998) J Phys Chem A 102:7041–7052
72. Leffler JE (1953) Science 117:340–341
73. Hammond GS (1955) J Am Chem Soc 77:334–338
74. Gilli G, Belluci F, Ferretti V, Bertolesi V (1989) J Am Chem Soc 111:1023–1028
75. Gilli G, Gilli P (2000) J Mol Struct 552:1–15
76. Krygowski TM, Zachara JE, Moszynski R (2005) J Chem Inf Model 45:1837–1841
77. Scheiner S (1994) Acc Chem Res 27:402–408
78. Filarowski A, Koll A (1996) Vibr Spectrosc 12:15–24
79. Filarowski A, Koll A, Glowiak T (2002) J Mol Struct 615:97–108
80. Rozas I, Alkorta I, Elguero J (2000) J Am Chem Soc 122:11154–11161
81. Cremer D, Kraka E (1984) Angew Chem Int Ed Engl 23:627–628
82. Grabowski SJ, Sokalski WA, Dyguda E, Leszczynski J (2006) J Phys Chem B 110:6444–6446
83. Grabowski SJ (2007) In: Matta CF, Boyd RJ (eds) The Quantum Theory of Atoms in Molecules:Relationships between QTAIM and the decomposition of the ınteraction energy-comparison of different kinds of hydrogen bond. Wiley, Weinheim, pp 453–469
84. Masui H (2001) Coord Chem Rev 219:957–992
85. Evangelio E, Ruiz-Molina D (2005) Eur J Inorg Chem 2957-2971
86. Karabiyik H, Erdem O, Aygun M, Guzel B, Garcia-Granda S (2010) J Inorg Organomet Polym 20:142–151